AGU PUBLICATIONS

JGR

Journal of Geophysical Research: Oceans

RESEARCH ARTICLE

10.1002/2017JC012731

Key Points:
- Wave decay over a model seagrass bed was measured in experiments that also involved blade motion imaging
- The reduction in wave-energy dissipation due to vegetation motion depends on the Cauchy number
- Scaling laws describing individual blade behavior are able to predict the reduction in wave decay over the meadow

Supporting Information:
- Supporting Information S1
- Movie S1
- Movie S2

Correspondence to:
M. Luhar,
luhar@usc.edu

Citation:
Luhar, M., E. Infantes, and H. Nepf (2017), Seagrass blade motion under waves and its impact on wave decay, *J. Geophys. Res. Oceans, 122*, doi:10.1002/2017JC012731.

Received 24 JAN 2017
Accepted 9 APR 2017
Accepted article online 13 APR 2017

Seagrass blade motion under waves and its impact on wave decay

M. Luhar[1], E. Infantes[2], and H. Nepf[3]

[1]Department of Aerospace and Mechanical Engineering, University of Southern California, Los Angeles, California, USA, [2]Department of Marine Sciences, University of Gothenburg, Gothenburg, Sweden, [3]Department of Civil and Environmental Engineering, Massachusetts Institute of Technology, Cambridge, Massachusetts, USA

Abstract The hydrodynamic drag generated by seagrass meadows can dissipate wave-energy, causing wave decay. It is well known that this drag depends on the relative motion between the water and the seagrass blades, yet the impact of blade motion on drag and wave-energy dissipation remains to be fully characterized. In this experimental study, we examined the impact of blade motion on wave decay by concurrently recording blade posture during a wave cycle and measuring wave decay over a model seagrass meadow. We also identified a scaling law that predicts wave decay over the model meadow for a range of seagrass blade density, wave period, wave height, and water depth scaled from typical field conditions. Blade flexibility led to significantly lower drag and wave decay relative to theoretical predictions for rigid, upright blades. To quantify the impact of blade motion on wave decay, we employed an effective blade length, l_e, defined as the rigid blade length that leads to equivalent wave-energy dissipation. We estimated l_e directly from images of blade motion. Consistent with previous studies, these estimates showed that the effective blade length depends on the dimensionless Cauchy number, which describes the relative magnitude of the wave hydrodynamic drag and the restoring force due to blade rigidity. As the hydrodynamic forcing increases, the blades exhibit greater motion. Greater blade motion leads to smaller relative velocities, reducing drag, and wave-energy dissipation (i.e., smaller l_e).

1. Introduction

Seagrasses are often termed ecosystem engineers because of their ability to alter local hydrodynamic conditions. Because seagrasses are a source of drag, they reduce near-bed water flow, and dissipate current-energy and wave-energy. In addition to serving as shelter for fauna, the low-flow environment within seagrass beds also leads to reduced sediment resuspension and increased sediment retention [e.g., *Gacia et al*., 1999; *Duarte et al*., 1999; *Granata et al*., 2001]. For example, *Fonseca et al*. [1983] observed that finite patches of seagrass were associated with local maxima in bed elevation in conditions with both current and waves, and attributed this effect to enhanced particle retention within the meadow. In addition to reducing flow locally, regionally the drag generated by seagrasses can lead to significant wave decay [*Fonseca and Cahalan*, 1992]. Smaller waves lead to lower near-bed flows, which could play an important role in reducing shoreline erosion.

Wave attenuation by submerged vegetation (including salt marsh vegetation and kelp forests) has been studied in the laboratory [e.g., *Fonseca and Cahalan*, 1992; *Kobayashi et al*., 1993; *Augustin et al*., 2009; *Sánchez-González et al*., 2011; *Stratigaki et al*., 2011; *Paul et al*., 2012; *Anderson and Smith*, 2014], in the field [e.g., *Knutson et al*., 1982; *Elwany et al*., 1995; *Mork*, 1996; *Coops et al*., 1996; *Möller et al*., 1999; *Bradley and Houser*, 2009; *Riffe et al*., 2011; *Infantes et al*., 2012], and using analytical methods or numerical models [e.g., *Kobayashi et al*., 1993; *Asano et al*., 1992; *Méndez et al*., 1999; *Méndez and Losada*, 2004; *Peterson et al*., 2004; *Chen et al*., 2007]. Most of these studies recognize that it is the relative motion between water and vegetation that sets drag. Yet, a number of these studies ignore the motion of the vegetation, which can lead to large errors in the estimation of wave damping. For example, if the blade tip follows the wave passively, it generates no drag.

In their analytical study, *Méndez et al*. [1999] accounted for plant motion by imposing a blade excursion that increased linearly with height, and used the resulting relative velocity to calculate drag. In a field study,

Bradley and Houser [2009] accounted for blade motion by recording the movement of seagrass blade tips from above and translating the measured tip excursion into blade motion over the entire blade height using a cantilever model. Although blade motion at the top of the meadow was significant in this study, wave decay was still predicted reasonably well with a rigid blade model. *Bradley and Houser* [2009] attributed this to the fact that the blades were moving in response to a broad wave spectrum, and so the resulting blade motion was out of phase with the peak wave frequency. Other studies [e.g., *Méndez and Losada*, 2004; *Sánchez-González et al*., 2011; *Infantes et al*., 2012] have employed bulk drag or friction coefficients that are calibrated to account for vegetation motion.

In recent years, there has been an increasing emphasis on quantifying the effect of vegetation flexibility on bending and motion, and the effect of this bending and motion on wave damping. For example, *Mullarney and Henderson* [2010] developed an analytical dynamic model for single-stem salt marsh vegetation under wave forcing, assuming that the stems can be modeled using linearized beam theory and that the hydrodynamic forcing is dominated by drag (i.e., inertial effects such as added mass do not play a role). Following on from this study, *Riffe et al*. [2011] measured the dissipation of waves over salt marsh vegetation and found that the rate of dissipation was about half that expected over rigid vegetation. However, the predicted dissipation rates were much closer to the observations when the model developed by *Mullarney and Henderson* [2010] was used to account for vegetation motion.

While models based on linear beam theory are reasonable for relative stiff salt marsh vegetation that undergoes limited bending in response to flow, such models may not apply for more flexible vegetation (e.g., seagrass) that experiences substantial bending and motion. With this in mind, *Luhar and Nepf* [2016] developed a more complete numerical model for the wave-induced dynamics of flexible blades that accounts for large deformations as well as inertial effects, and validated this model via laboratory experiments. This study showed that blade motion is governed primarily by two dimensionless parameters: (i) the Cauchy number, *Ca*, which represents the relative magnitude of the hydrodynamic forcing to the restoring force due to blade stiffness, and (ii) the ratio of blade length to wave orbital excursion, *L*. For large wave excursions ($L \ll 1$), the flow resembles a unidirectional current and the scaling laws developed in previous steady-flow reconfiguration studies [*Alben et al*., 2002; *Gosselin et al*., 2010; *Luhar and Nepf*, 2011] should apply. For small excursions ($L \gg 1$), the beam equations may be linearized and the model developed by *Mullarney and Henderson* [2010] holds. Further, *Luhar and Nepf* [2016] showed that the small-excursion scaling laws apply even for intermediate cases with $L \sim O(1)$.

The present paper builds on these recent advances in our ability to model wave-vegetation interaction by providing a thorough examination of the effects of blade motion on wave damping. In particular, the laboratory study described below is unique in that it provides detailed observations of blade posture and blade motion over the entire length of the blade for a submerged flexible meadow, designed to mimic the seagrass *Zostera marina*, interacting with progressive waves. By observing blade motion over the entire blade length, the experiments offer new insight into the vertical distribution of wave drag in a meadow and its impact on wave damping. In addition, the stem density, wave period, amplitude, and water depth are varied systematically over a parameter range comparable to that observed in the field to elucidate the impact of each variable on wave decay. Broadly, our results show that the dimensionless framework developed by *Luhar and Nepf* [2016] for individual blades adequately accounts for the effect of blade motion on wave decay at the canopy-scale. Finally, for field application, we also consider the impact of submerged vegetation at the regional scale by calculating the ratio of the steady state wave heights for wind-generated waves over a vegetated bed relative to a sandy bed.

2. Theory

2.1. Wave-Energy Dissipation

For the wave decay analysis, we follow the model proposed by *Dalrymple et al*. [1984]. Assuming linear wave theory is valid and that energy dissipation in the seagrass meadow alone is responsible for wave decay, the steady state energy balance for monochromatic waves is given by:

$$\frac{\partial}{\partial x}\left(\frac{1}{2}\rho g a^2 c_g\right) = -E_D. \tag{1}$$

Here x is the direction of wave propagation, ρ is the density of the water, g is the acceleration due to gravity, a is the wave amplitude, c_g is the wave group speed, and E_D is the rate of energy dissipation per unit bed area due to the presence of the vegetation. Using a standard quadratic drag law, E_D can be expressed as:

$$E_D = \frac{1}{T}\int_0^T \int_0^l \frac{1}{2}\rho C_D a_v |u_R| u_R u \, dz \, dt. \tag{2}$$

The parameter a_v is the vegetation frontal area per unit volume, C_D is the drag coefficient, u_R is the *relative* horizontal velocity between the vegetation and the water, u is the absolute water velocity, l is the blade length, and T is the wave period. Note that z represents the vertical coordinate ($z = 0$ at the bed) and t denotes time.

A number of assumptions have been made to yield (2). Following previous researchers [*Dalrymple et al.*, 1984; *Méndez and Losada*, 2004; *Bradley and Houser*, 2009], inertial forces due to the relative acceleration of water and vegetation have been ignored. This is a reasonable assumption since inertial forces tend to be out of phase with water velocity, causing little dissipation over a wave cycle. Given the morphology of seagrasses (tall, thin blades), the vertical drag force is also assumed to be negligible compared to the horizontal drag force. This assumption breaks down as the blades get pushed over into a bent posture. We account for this inconsistency below in section 3.

If the wave-induced velocities are adequately described by linear wave theory, the horizontal velocity is:

$$u = a\omega \frac{\cosh kz}{\sinh kh} \sin \omega t, \tag{3}$$

and the vertical velocity is

$$w = a\omega \frac{\sinh kz}{\sinh kh} \cos \omega t. \tag{4}$$

Here $\omega = 2\pi/T$ is the wave radian frequency, $k = 2\pi/\lambda$ is the wave number (λ is wavelength), and h is water depth. The dispersion relation $\omega^2 = kg\tanh(kh)$ describes the relationship between wave frequency and wave number.

For rigid vegetation, the relative velocity between the vegetation and the water is identical to the absolute fluid velocity, $u_R = u$. At this limit, (2) can be integrated and substituted into (1) to yield (assuming C_D and a_v are constant)

$$\frac{\partial}{\partial x}\left(\frac{1}{2}\rho g a^2 c_g\right) = -\frac{2}{3\pi}\rho C_D a_v \left(\frac{a\omega}{\sinh kh}\right)^3 \left[\frac{9\sinh kl + \sinh 3kl}{12k}\right], \tag{5}$$

which has a solution of the form

$$\frac{a}{a_0} = \frac{1}{1 + K_D a_0 x}. \tag{6}$$

Here a_0 is the initial wave amplitude at $x = 0$ (defined as the start of the meadow) and K_D is a constant, defined as

$$K_D = \frac{2ka_v}{9\pi} C_D \left[\frac{9\sinh kl + \sinh 3kl}{\sinh kh(\sinh 2kh + 2kh)}\right]. \tag{7}$$

Note that using a quadratic drag law does not lead to exponential wave decay, which is the fitting model used most frequently for wave decay analyses. However, for small $K_D a_0 x$, the behavior is very similar. Specifically, $\exp(-K_D a_0 x) \approx (1 + K_D a_0 x)^{-1}$ for $K_D a_0 x < 0.5$. Throughout this paper, we use the dimensionless parameter $K_D a_0 \lambda$ to represent wave decay. This dimensionless parameter quantifies the relative decay in wave amplitude over a distance equal to the wavelength. From (7), this dimensionless wave decay rate can be expressed as:

$$K_D a_0 \lambda = \frac{4 a_v a_0}{9} C_D \left[\frac{9 \sinh kl + \sinh 3kl}{\sinh kh (\sinh 2kh + 2kh)} \right]. \quad (8)$$

For flexible vegetation that moves in response to flow, the drag force in (2) must be calculated based on the relative velocity. Previous studies have employed simplified cantilever models (i.e., models based on linear beam theory) for blade motion to estimate relative velocities [*Bradley and Houser*, 2009; *Mullarney and Henderson*, 2010]. Our observations of blade motion, described below, suggest that a simple cantilever model may not be appropriate under all wave forcing, as the degree of blade curvature far exceeds the assumptions of linear beam theory. To quantify the impact of blade motion on wave decay, we employ an effective blade length l_e, which is defined as the rigid blade length that dissipates the same wave-energy as the moving flexible blade. Under these assumptions, (5)–(8) remain valid but l is replaced by the effective length l_e. We estimate this effective length directly from blade posture images captured over a wave cycle. This is described in section 3. The dependence of blade motion, and specifically l_e, on the forces acting on the blade is considered in section 2.2 below.

Finally, by assuming that the fluid velocity over the entire water depth is given by linear wave theory, we ignore the possible reduction of wave-induced velocity within the meadow. *Lowe et al*. [2007] show that wave-induced velocities may be reduced significantly within vegetated canopies if the horizontal wave excursion, A, is much longer than the drag length scale of the vegetation, given by a_v^{-1}. The reduction of wave-induced velocity within the meadow can have a major impact on energy dissipation within the meadow, which is proportional to $|u|u^2$. For the majority of the experimental runs presented in this paper, the wave excursion is shorter than the drag length scale. As a result, the wave-induced velocity is not significantly diminished within the meadow, as shown in *Luhar et al*. [2010]. However, we keep this limit in mind when interpreting our experimental results for field application.

2.2. Blade Motion and Effective Length

As noted above, to account for the effect of blade motion on drag and wave decay, we employ an effective blade length l_e. *Luhar and Nepf* [2016] show that this effective blade length depends primarily on two dimensionless parameters: (i) the Cauchy number, Ca, and (ii) the ratio of blade length to wave excursion, L. Here we provide a brief review of the scaling laws for effective length identified in *Luhar and Nepf* [2016].

The Cauchy number is defined as:

$$Ca = \frac{\rho b U^2 l^3}{EI}, \quad (9)$$

in which b is the blade width, U is a characteristic wave-velocity scale (assumed to be the magnitude of u at the bed (3)), E is the elastic modulus of the blade, and $I = bd^3/12$ is the second moment of area for the blade cross-section, where d is blade thickness. The length ratio is defined as:

$$L = \frac{l}{A}, \quad (10)$$

where $A = U/\omega$ is the wave orbital excursion.

When the drag associated with wave forcing is much smaller than the restoring force due to stiffness, $Ca \ll 1$, the blade remains upright in the flow. At this effectively rigid limit, the hydrodynamic drag generated by the blade is predicted well by assuming a typical flat plate drag coefficient. However, as the wave forcing increases such that $Ca > O(1)$, the blade begins to bend and move in response to the wave. The resulting reduction in drag depends on the length ratio L.

At the limit of large wave excursion ($L \ll 1$), we have a quasi steady situation in which a flexible blade can be pushed over into a bent posture in the early stages of a wave half-cycle (see Figure 1a). The blade remains bent until the oscillatory flow reverses direction. The bent posture held during most of the wave cycle reflects a balance between the restoring force due to stiffness and the hydrodynamic drag. In this reconfigured state, the restoring force due to stiffness scales as $EI(\partial^2\theta/\partial s^2) \sim EI(1/l_e^2)$, in which θ is the local blade angle relative to the vertical and s is the distance along the blade (Figure 2). Similarly, the drag force scales as $F_x \sim \rho b l_e U^2$. In other words, both the blade curvature and the drag depend on the effective

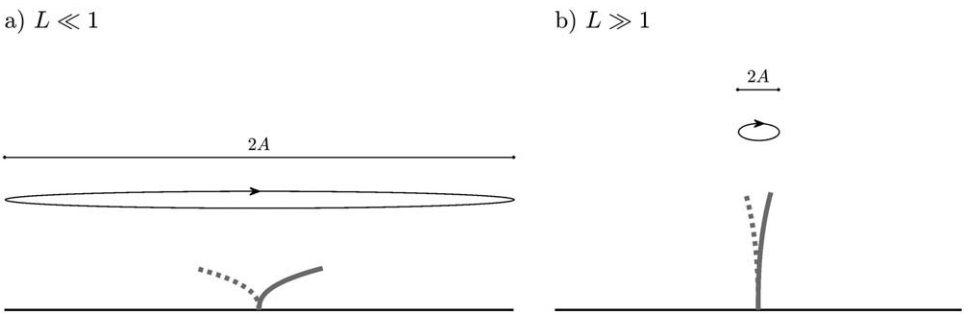

Figure 1. Schematic illustrating the difference in blade behavior at (a) the large-excursion limit ($L \ll 1$) and (b) the small-excursion limit ($L \gg 1$). This figure is modified from *Luhar and Nepf* [2016].

length in the reconfigured state. This balance between stiffness and drag, $EI(1/l_e^2) \sim \rho b l_e U^2$, can be rearranged to yield the following scaling law:

$$\frac{l_e}{l} \sim Ca^{-1/3}. \tag{11}$$

This scaling law is identical to that found for reconfiguration in *steady* flow (first proposed by *Alben et al.* [2002]).

At the limit of small wave excursions ($L \gg 1$), we anticipate that the blade remains nearly vertical as it oscillates back and forth over a wave cycle, and that the horizontal excursion of the blade scales with the wave excursion (Figure 1b). For this small-deflection limit, the blade curvature term can be linearized such that $\partial^2\theta/\partial s^2 \approx \partial^3 x_v/\partial z_v^3$, in which x_v and z_v are the local horizontal and vertical coordinates along the blade (Figure 2). Since the blade horizontal excursion scales on the wave excursion, $|x_v| \sim A$, balancing blade stiffness and drag for this small-excursion limit yields $EI(A/l_e^3) \sim \rho b l_e U^2$. Using the definition of Ca and L, this balance can be rewritten as:

$$\frac{l_e}{l} \sim (CaL)^{-1/4}. \tag{12}$$

With this scaling, the effective length l_e represents the length over which there is significant relative motion between the blade and the water. The upper part of the blade moves nearly passively with the flow, contributing negligible drag. Note that this small-deflection behavior is identical to that described in the analytical model developed by *Mullarney and Henderson* [2010].

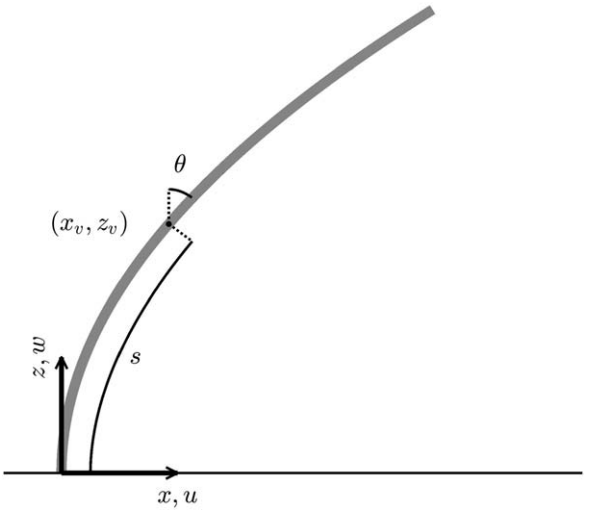

Figure 2. Schematic showing the coordinate system used to estimate blade posture, velocity, and drag.

The scaling laws shown in (11) and (12) both assume that drag is the dominant hydrodynamic forcing. For wave-induced oscillatory flows, inertial effects such as added mass can also be important. The drag force per unit blade length is expected to scale as $\rho b U^2$, while added mass is expected to scale as $\rho b^2 U\omega$ [*Vogel*, 1994]. Thus, the Keulegan-Carpenter number, $KC = UT/b$, which is the ratio of wave orbital excursion to the blade width [*Keulegan and Carpenter*, 1956; *Graham*, 1980], can be used to assess the relative magnitude of drag and inertial effects. For the conditions tested in the present study, $KC \geq 11$ (Table 1), and so inertial effects are expected to be less important than drag.

Further, the scaling laws also neglect the influence of blade buoyancy. The relative

Table 1. Table Listing the Wave and Vegetation Parameters for the Experiments[a]

	n (m^{-2})	h (cm)	T (s)	a_0 (cm)	λ (cm)	$a_v l$	l/h	kh	a_0/h	Re	KC	Ca	L	l_e/l
D1	1800	39	1.4	3.0	240	0.7	0.3	1.0	0.08	330	52	1030	5.3	
D2	3600	39	1.4	3.3	240	1.4	0.3	1.0	0.09	360	58	1300	4.7	
D3	5400	39	1.4	3.0	240	2.1	0.3	1.0	0.08	330	52	1050	5.2	
D4[b,c]	7200	39	1.4	3.4	240	2.8	0.3	1.0	0.09	370	59	1330	4.6	0.21
D5	9000	39	1.4	3.2	240	3.5	0.3	1.0	0.08	350	55	1180	4.9	
D6	10800	39	1.4	2.8	240	4.2	0.3	1.0	0.07	310	49	910	5.6	
H1	7200	16	1.4	1.4	170	2.8	0.8	0.6	0.09	290	47	850	5.8	
H2	7200	24	1.4	2.0	210	2.8	0.5	0.7	0.08	330	53	1070	5.2	
H3	7200	32	1.4	2.6	230	2.8	0.4	0.9	0.08	350	55	1170	4.9	
H4[b,c]	7200	39	1.4	3.4	240	2.8	0.3	1.0	0.09	370	59	1330	4.6	0.21
T1	7200	39	0.8	3.6	90	2.8	0.3	2.7	0.09	120	11	150	25.9	
T2[b]	7200	39	0.9	2.7	125	2.8	0.3	2.0	0.07	160	16	260	16.5	0.35
T3[b]	7200	39	1.1	3.7	170	2.8	0.3	1.4	0.09	310	39	970	7.0	0.21
T4[b,c]	7200	39	1.4	3.4	240	2.8	0.3	1.0	0.09	370	59	1330	4.6	0.21
T5[b]	7200	39	2.0	3.5	370	2.8	0.3	0.7	0.09	460	102	2060	2.7	0.23
A1[b]	7200	39	1.4	0.9	240	2.8	0.3	1.0	0.02	100	16	100	17.1	0.40
A2	7200	39	1.4	1.9	240	2.8	0.3	1.0	0.05	210	33	420	8.2	
A3[b,c]	7200	39	1.4	3.4	240	2.8	0.3	1.0	0.09	370	59	1330	4.6	0.21
A4	7200	39	1.4	4.8	240	2.8	0.3	1.0	0.12	530	84	2710	3.3	
A5[b]	7200	39	1.4	5.6	240	2.8	0.3	1.0	0.14	610	97	3610	2.8	0.20
	[30]	[0.5]	[0.05]	[0.2]	[5]									[0.03]

[a]Runs D1–D6 measure wave decay over a range of vegetation densities. Similarly, H1–H4 vary water depth, T1–T5 vary wave period while A1–A5 vary wave amplitude. The final row indicates typical uncertainty for each variable.
[b]Blade motion was tracked for these runs, yielding direct measurement of l_e via (15).
[c]D4, H4, T4, and A3 are identical runs listed in multiple locations for ease of comparison.

magnitude of the restoring force due to buoyancy and the restoring force due to stiffness is denoted by the buoyancy parameter:

$$B = \frac{(\rho - \rho_v) g b d l^3}{EI}, \tag{13}$$

in which ρ_v is the blade material density. *Luhar and Nepf* [2011] show that for steady flows with $B \gg 1$, the additional restoring force due to buoyancy can delay the onset of reconfiguration. Specifically, the blade does not begin to bend until the hydrodynamic forcing is large enough to overcome buoyancy, $Ca > O(B)$. However, once the hydrodynamic forcing exceeds the buoyancy force, $Ca \gg B$, the scaling law shown in (11) applies. For further discussion on why buoyancy does not alter (11), the reader is referred to *Luhar and Nepf* [2011]. Thus, buoyancy could delay the onset of bending for the quasi steady large-excursion limit illustrated in Figure 1a without affecting the eventual scaling law shown in (11). On the other hand, for the small-deflection limit shown in Figure 1b, buoyancy is unlikely to be play a major dynamic role. This is because blade motion is dictated primarily by the balance of forces acting perpendicular to the blade. At the limit where $L \gg 1$, the blades remain nearly upright and so the effect of buoyancy would only affect the force balance along the blade, i.e., in the vertical direction. For all the laboratory experiments discussed below, $Ca \gg B$ and $L \geq 2.7$ (Table 1). For these high forcing conditions with relatively small wave excursions, we do not expect buoyancy effects to be important.

3. Experimental Methods

Laboratory experiments were carried out in a 24 m long, 38 cm wide, and 60 cm high wave channel (Figure 3) in the Environmental Fluid Mechanics Laboratory at MIT. Waves were generated at the upstream end of the channel by a vertical paddle driven by a hydraulic piston. The motion of the paddle was controlled by a Syscomp WGM-101 arbitrary waveform generator programmed to produce surface waves of a desired frequency and amplitude, based on the closed form solution developed by *Madsen* [1971]. A plywood beach with layers of rubberized coconut fiber was installed on the downstream end of the channel. The beach reflected less than 10% of the wave-energy.

The model seagrass meadow was constructed using artificial plants (Figure 4) that were geometrically and dynamically similar to seagrasses such as *Zostera marina* (eelgrass) and *Posidonia oceanica*, as described by *Ghisalberti and Nepf* [2002]. Each shoot consisted of a 2.0 cm long basal stem (made from a circular cylinder)

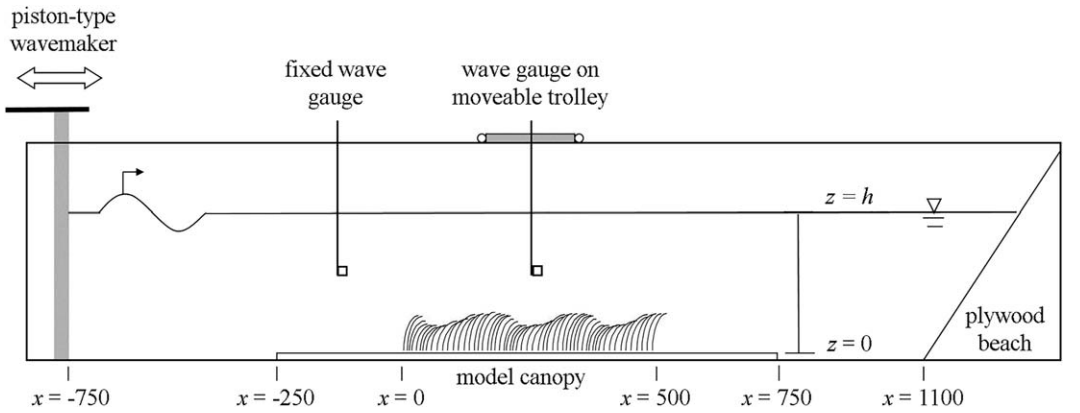

Figure 3. Schematic showing a side view of the wave channel (all dimensions cm; not to scale). The direction of wave propagation, as indicated by the arrow, is from left to right. Baseboards were put in place for the region 2.5 m upstream and 2.5 m downstream of the model seagrass canopy to ensure that any measured wave transformation was due to the vegetation alone. The slope of the plywood beach is 1:5.

and six blades. The blades were attached to the basal stem using a rubber band, which locally increased the diameter. The extent of the overlap between the stem and the blades was 1.0 cm. The stem diameter, d_s, will be defined as the average between the minimum (6.4 mm) and maximum (9.2 mm) measured diameters of a typical stem, i.e., d_s=7.8 mm. The blades were cut from low-density (ρ_v=920 kg m^{-3}) polyethylene film with a modulus of elasticity, E=3.0×10^8 Pa. The blades were l = 13 cm long (excluding 1 cm stem overlap), b = 3 mm wide, and d = 0.1 mm thick. The buoyancy parameter (13) for these blades is B = 6.9.

A random algorithm was used to place the stems in predrilled baseboards at stem densities ranging from 300 to 1800 stems m^{-2} (blade densities, n = 1800–10,800 m^{-2}). Only the top 1.0 cm of the stems, the region attached to the blades, protruded above the baseboards. The blade density was chosen based on field observations of *Zostera marina* and *Posidonia oceanica* [*Moore*, 2004; *Marbà et al*., 2005; *Luhar et al*., 2010]. The frontal area per unit volume for the blades, a_v=nb, ranged from 0.054 to 0.32 cm^{-1}. These densities correspond to a blade frontal area index $a_v l \approx 0.7$ to 4.2. Field meadows for eelgrass have been observed in the range $a_v l \approx 0.3$ to 1.1, based on biomass data from *Moore* [2004], converted to frontal area index in *Luhar et al*. [2008]. For species such as *Posidonia oceanica*, the frontal area index can be as high as $a_v l \approx 4$ [based on data from *Pergent-Martini et al*., 1994].

To achieve similarity in wave conditions, the following dimensionless parameters were matched to field conditions: kh (the ratio of wavelength to water depth), and l/h (blade length to water depth). Most seagrass species (>75%) are found in less than 20 m depth [*Duarte*, 1991] and are affected by wave peak periods from 0.6 to 15 s [*Ward et al*., 1984; *Koch et al*., 2006; *Bradley and Houser*, 2009]. Based on these conditions, we chose values of kh ranging from 0.6 to 2.7 and l/h ranging from 0.3 to 0.8, which represent the shallow region of a seagrass meadow. For example, assuming blades of length $l \approx 1$ m [*Luhar et al*., 2013; *Eriander et al*., 2016], kh = 0.6 and l/h=0.3 correspond approximately to waves of period 6 s in 3 m water depth; kh = 2.7 corresponds approximately to waves of period T = 2 s. Similarly, the typical amplitude ratio employed in the experiments (Figure 3), $a_0/h \approx 0.1$ scales to waves of amplitude 30 cm in 3 m water depth. The length of the

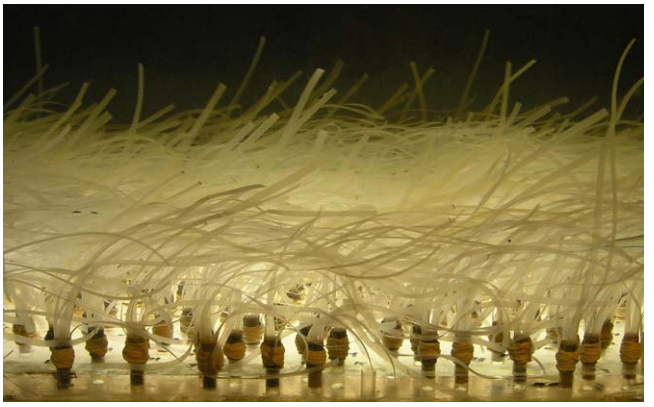

Figure 4. Photo of the model canopy with wave approaching from the left. The seagrass density is 1800 stems m^{-2}. The stem protrudes approximately 1 cm above the baseboards into the water. The mean measured diameter of the stems was d = 7.8 mm.

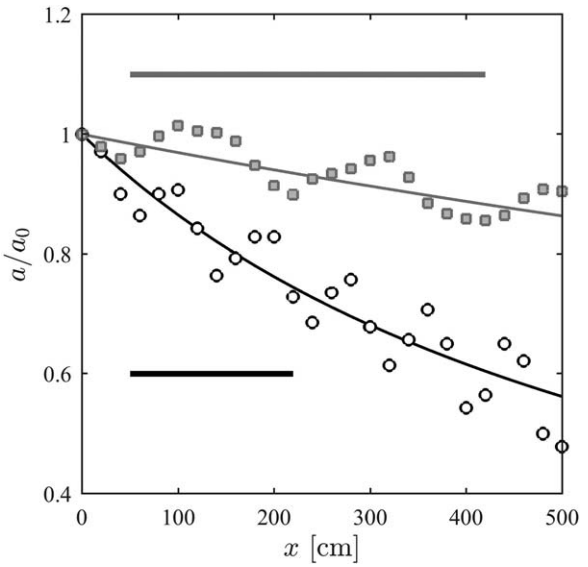

Figure 5. Wave amplitude measurements for runs H1 (a_0=1.4 cm, T = 1.4 s, h = 16 cm; open black circles) and T5 (a_0=3.5 cm, T = 2.0 s, h = 39 cm; filled gray squares). The best fit decay curves for these measurements correspond to $K_D a_0 \lambda$=0.26 for run H1 (fine black line) and $K_D a_0 \lambda$=0.12 (fine gray line) for run T5. The heavy gray line shown above the measurements indicates the wavelength for run T5 (λ = 370 cm) and the heavy black line shown below the measurements indicates the wavelength for run H1 (λ = 170 cm). The oscillation in measured wave amplitudes reflects the partially standing wave created due to downstream reflection; as a result it is periodic with a spatial scale of $\lambda/2$.

model meadow, 500 cm, was 1.4–5.5 times the wavelength λ. The leading edge of the meadow is denoted $x = 0$.

The wave parameters for each individual experiment are listed in Table 1. For reference, the wave period ranged from T = 0.8 to 2.0 s (Runs T1–T5), the wave amplitude upstream of the meadow ranged from a_0=0.9 to 5.6 cm (Runs A1–A5), and the water depth ranged from h = 16 to 39 cm (Runs H1–H4). Table 1 also lists the Reynolds number based on blade width ($Re = Ub/\nu = 100-610$, where ν is the kinematic viscosity of water), the Keulegan-Carpenter number ($KC = 11-102$), the Cauchy number ($Ca = 100-3610$), and ratio of blade length to wave excursion ($L = 2.7-25.9$) for each case.

The wave amplitude was measured using two resistance-type wave gauges with 0.2 mm accuracy. One wave gauge was permanently mounted at x = 125 cm to provide a reference measurement verifying that the wave conditions were constant throughout the experimental run. The second wave gauge was mounted on a mobile trolley that moved on precision rails. The mobile gauge was used to measure wave records at 20 cm intervals from 40 cm upstream of the meadow and continuing along its entire length. At each x position, the instantaneous position of the water surface was measured at 25 Hz for 120 s (60–132 waves, depending on wave frequency). The surface displacement measurements were binned into 25 T phase groups (e.g., 50 phase groups for waves of period T = 2.0 s) based on the zero-crossings of the record, and averaged, yielding a phase-averaged waveform $\eta(t)$. The wave amplitude was calculated based on the root mean squared value of the phase-averaged waveform:

$$a = \sqrt{\frac{2}{T}\int_0^T \eta^2(t)\,dt}. \tag{14}$$

Equation (6) was then fitted to the wave amplitude measurements to obtain the decay parameter $K_D a_0 \lambda$ for each experiment. As an example, the measured wave amplitudes and fitted decay curves for runs H1 (a_0=1.4 cm, T = 1.4 s, h = 16 cm, see Table 1) and T5 (a_0=3.5 cm, T = 2.0 s, h = 39 cm) are shown in Figure 5. The major source of error for the wave decay fits was the partially standing wave created in the flume because of reflections (<10%) from the downstream end. Due to this standing wave, the measured wave amplitude exhibited small oscillations, periodic at a spatial scale of half the wavelength (Figure 5). Note that wave-energy is also dissipated in the laminar boundary layers at the flume bed and sidewalls due to viscosity. To correct for this, we subtracted the theoretical viscous decay per wavelength [*Hunt*, 1964] from the fitted decay parameter. This correction typically resulted in a relative reduction of less than 10% for the fitted value of $K_D a_0 \lambda$.

Blade motion was recorded in images taken midway along the meadow at 15 Hz using a Sony DFW-X710 CCD camera. Images were taken for the wave conditions marked with an asterisk in Table 1, but with a lower density (n = 1800 blades m^{-2}) for better image clarity. One of the blades was marked with a red dot at 2 cm intervals along the blade and the marks were tracked over five wave cycles. Neighboring blades moved in near-unison, hence tracking a single blade was sufficient to characterize blade motion (see movies in supporting information). A fifth-order polynomial fit to the marked positions was used to estimate the

blade position and angle to the vertical (x_v, z_v, and θ in Figure 2) as a function of distance along the blade, s, at different phases in the wave cycle. Sinusoidal curves were fitted to the observed blade positions over a wave cycle to obtain the horizontal and vertical blade velocities ($\partial x_v/\partial t$, $\partial z_v/\partial t$). At higher stem densities, there was some interference between neighboring blades for certain wave conditions. The nature of this interference and potential implications for blade motion tracking are discussed in section 4.1.

The observed blade velocities were used together with the horizontal (3) and vertical (4) orbital velocities predicted by linear wave theory to calculate relative velocities, $u_R = u - (\partial x_v/\partial t)$ and $w_R = w - (\partial z_v/\partial t)$. For all the wave conditions considered in this study, vertical profiles of velocity measured upstream of the meadow were within 95% of predictions made by linear theory [*Luhar et al.*, 2010]. The rate of energy dissipation within the meadow was then estimated using the equation:

$$E_D = \frac{1}{T}\int_0^T \int_0^l \frac{1}{2}\rho C_D a_v |u_{RN}| u_{RN} u_N \, ds \, dt, \tag{15}$$

where $u_{RN} = u_R \cos\theta - w_R \sin\theta$ is the relative velocity normal to the blade, and $u_N = u\cos\theta - w\sin\theta$ is the fluid velocity normal to the blade. As shown in Figure 2, θ is the angle of the blade relative to vertical, and so (15) accounts for the bent posture of the blades by considering both horizontal and vertical relative velocities. To estimate the effective blade length, the rate of energy dissipation calculated using (15) was equated with the expression shown on the right-hand side of equation (5), replacing l with l_e in equation (5). This method of estimating the effective blade length requires the further assumptions that C_D and a_v are constant in time and in position along the blade, so that the factor $C_D a_v$ cancels when equating (5) and (15). Note that in the limit of rigid, upright vegetation ($\theta = 0$, $u_{RN} = u_R = u$), (15) is identical to the expression shown in (2).

4. Results

4.1. Blade Posture and Motion

Movies of blade motion showed behavior that followed or fell between the two cases illustrated in Figure 6. This figure shows the fitted blade posture at six equally spaced phases of a wave cycle for wave conditions corresponding to the lowest amplitude case A1 ($a_0 = 0.9$ cm, $T = 1.4$ s, $h = 39$ cm) and the highest amplitude case A5 ($a_0 = 5.6$ cm, $T = 1.4$ s, $h = 39$ cm). Curves marked 1, 2, and 3 show blade posture under the wave crest (forward stroke) while curves 4, 5, and 6 show motion under the wave trough (return stroke). For both runs, the horizontal excursion of the blade tips was comparable to the wave excursion. However, blade motion under the return stroke varied dramatically for the two cases.

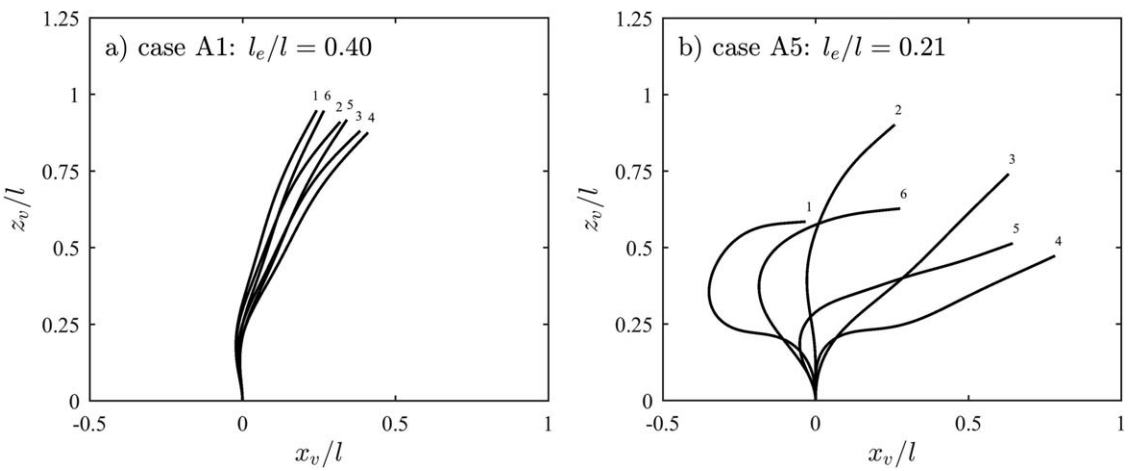

Figure 6. (a) Blade posture at six different phases during a cycle for wave conditions corresponding to case A1. Curves 1, 2, and 3 indicate blade posture during the passage of a wave crest while curves 4, 5, and 6 show posture under a wave trough. (b) Blade posture for wave conditions corresponding to case A5. Also shown on the plots is the estimated effective blade length l_e calculated using (15). Movies of blade motion for cases A1 and A5 are included in supporting information.

For the wave conditions in run A1, the blade remained relatively upright as it moved throughout the wave cycle (Figure 6a). For this case, the effective blade length was estimated to be l_e/l=0.40, indicating that blade flexibility significantly reduced the drag (cutting it by more than half) relative to a rigid blade of comparable length. For high-amplitude wave conditions, the blade motion was more complex, with significant blade motion over most of the blade length (e.g., run A5, Figure 6b). The blade remained relatively still and upright only very close to the bed. Greater blade motion translated into smaller relative velocities, which led to a further reduction in the effective blade length relative to run A1, specifically the effective length was estimated to be l_e/l=0.21. Photographs from *Koch et al.* [2006] show blade postures in the field similar to those in Figure 6b, confirming the dynamic similarity between natural seagrass and the model employed for this study. Note that *Paul et al.* [2012] also observe broadly similar blade motion in their laboratory experiments.

We observed a net mass transport (unidirectional current) in the direction of wave propagation that extended vertically over the height of the seagrass meadow. This induced current is analogous to the steady streaming observed in wave boundary layers [for further detail, see *Luhar et al.*, 2010, 2013]. The magnitude of this steady streaming was large enough (as much as 8 cm s^{-1}) to create a bias in blade posture in the streamwise direction (Figure 6). However, the effective blade length calculated using (15) accounts for this bias in posture. (Biased blade postures have also been observed for single blades in oscillatory flows, though the exact mechanisms leading to this mean pronation remain to be fully understood [*Gijón Mancheño*, 2016; *Luhar and Nepf*, 2016].)

For the wave conditions in the intermediate amplitude case A3 (a_0=3.4 cm, T = 1.4 s, h = 39 cm), and the low-frequency case T5 (a_0=3.5 cm, T = 2.0 s, h = 39 cm), blade motion resembled the observed behavior for run A5 (high amplitude, Figure 6b). Blade motion for the high-frequency waves in experiment T2 (a_0=2.7 cm, T = 0.9 s, h = 39 cm) was similar to that observed for A1 (low amplitude, Figure 6a). The difference in blade motion is reflected in the effective blade lengths reported in Table 1. Note that the wave velocities were larger for experiments A3, A5, and T5 compared to experiments A1 and T2, suggesting that hydrodynamic forcing dictates blade motion and sets the effective length, with higher wave-induced velocities leading to smaller effective blade lengths. The relationship between effective length and hydrodynamic forcing is considered in greater detail in section 5.1.

The above image analysis was carried out for blade density n = 1800 blades m^{-2}. At higher stem density the reduced center-center spacing between the model plants led to interference between neighboring blades. Qualitative observations indicate that blade motion for high-frequency or low-amplitude waves did not change significantly. The relatively upright posture of the blades during these runs, similar to Figure 6a, ensured that there was little interference from neighboring blades. However, the complex blade motion seen for high-amplitude waves (Figure 6b) was affected. At densities above 7200 blades m^{-2}, the upper portions of the blades remained depressed in a streamwise posture throughout the wave cycle. The blades oscillated periodically between the postures shown by curves 4, 5, and 6 in Figure 6b, without undergoing the postures shown by curves 1, 2, and 3. This streamwise posture ensures that the upper portions of the blades provide very little flow resistance (only skin friction). Drag generation is again dominated by the lower part of the blades and hence, our earlier estimates of effective blade length remain valid.

4.2. Wave Decay

The measured wave decay, expressed as $K_D a_0 \lambda$, is shown in Figure 7 as a function of the dimensionless vegetation parameters $a_v l$, a_0/h, l/h, and kh. For reference, we also show curves (black lines in Figure 7) corresponding to the wave decay predicted for rigid, upright blades, i.e., $l_e = l$ in (8). For simplicity, we assume a constant value for the drag coefficient for these predictions, C_D=1.95, which corresponds to a flat plate normal to flow at high Reynolds number. In general, the drag coefficient is expected to vary both as a function of the Reynolds number, Re, and the Keulegan-Carpenter number, KC. For steady flows, the Reynolds number dependence can be approximated as $C_D \approx 1.95 + 50/Re$ [*Ellington*, 1991; *Vogel*, 1994]. For oscillatory flows at high Reynolds number, *Luhar and Nepf* [2016] suggested the following dependence $C_D = \max(1.95, 10KC^{-1/3})$ based on data from *Graham* [1980]. In the present experiments, the Keulegan-Carpenter number ranged from KC = 11 to 102, while the Reynolds number ranged from Re = 100 to 610 (Table 1). Based on the expressions given above, $C_D \approx 2.1-4.6$ over this parameter range. Thus, C_D=1.95 is likely to be an underestimate of the true drag coefficient, making the solid curves in Figure 7 an underestimate of the rigid

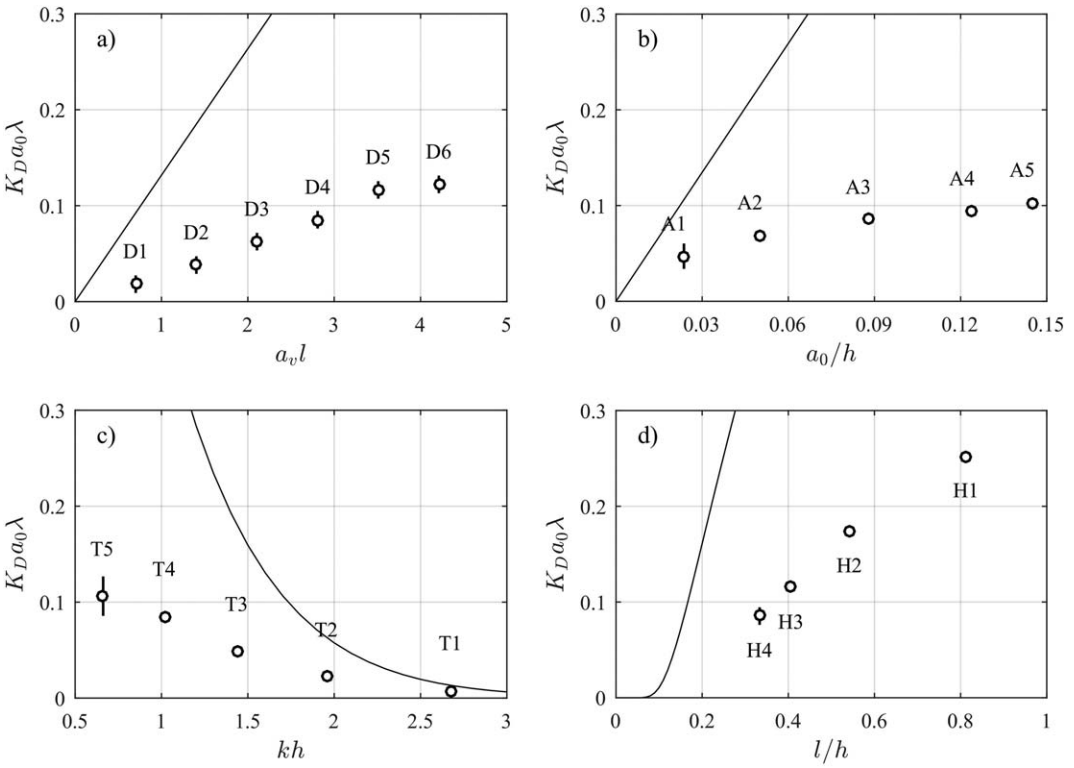

Figure 7. Measured wave decay per wavelength ($K_D a_0 \lambda$). (a) Experiments D1–D6: varying vegetation density, expressed as the dimensionless parameter $a_v l$, (b) experiments A1-A5: varying wave amplitude, plotted as a_0/h, (c) experiments T1–T5: varying wave period (and wavelength) expressed as kh, and (d) experiments H1–H4: varying water depth, plotted as l/h. For experiments D1–D6, A1–A5, and T1–T5, only one dimensionless parameter varies (e.g., for A1–A5, kh, l/h, and $a_v l$ are constant). For experiments H1–H4, however, both a_0/h (0.3–0.8) and kh (0.6–1.0) vary. See Table 1 for more detail. The solid lines show predicted decay based on (8) assuming $C_D = 1.95$ and $l_e = l$. The error bars represent 95% confidence limits on the fitted wave decay parameter $K_D a_0 \lambda$. The major source of error in all cases was wave reflection from the downstream end of the flume.

blade wave dissipation. Despite this underestimation, with the rigid blade assumption, (8) overpredicts wave decay for all the experimental runs, clearly showing that blade flexibility leads to reduced drag. Significantly, the rigid blade assumption overpredicts wave decay by a factor of more than 3 in most cases (Figure 7). Exceptions to this are the high-frequency cases, T1 and T2 shown in Figure 7c, and the low-amplitude cases, A1 and A2, shown in Figure 7b. For these cases, the rigid, upright blade assumption overpredicts wave decay by a factor of 2 to 3, consistent with the estimated effective blade lengths for runs T2 and A1 ($l_e/l \approx 0.4$, see Table 1). Further, the over prediction of wave decay by the rigid blade assumption increases with increasing wave amplitude (Figure 7b) and decreasing wave number (Figure 7c), which would correspond to increasing wavelength and period. In other words, the wave decay measurements suggest that an increase in orbital velocity, associated with a higher amplitude or longer period, leads to a decrease in effective blade length, consistent with the direct observations of blade posture and motion (Figure 6).

In addition to the drag reduction associated with flexible blades presented above, we also observed the following general trends in wave decay. Wave decay increased with vegetation density (Figure 7a), and the trend was approximately linear for the lower vegetation densities. However, wave decay reached a plateau for the two highest densities, Runs D5 ($n = 9000$ blades m^{-2}) and D6 ($n = 10{,}800$ blades m^{-2}) shown in Figure 7a. Lower decay may be explained based on the arguments put forth by *Lowe et al.* [2007]. As the orbital excursion approaches or exceeds the drag length scale ($A \sim a_v^{-1}$), the wave-induced flow within the meadow is damped, resulting in lower velocities. Lower in-canopy velocities lead to reduced energy dissipation (2) and wave decay. For run D5, the orbital excursion was $A = 2.7$ cm, and the drag length scale was $a_v^{-1} = 3.7$ cm, suggesting that the velocity damping limit was approached ($Aa_v = 0.7$ for D5 and $Aa_v = 0.8$ for D6). Thus, even though more drag elements were present in case D6, relative to case D5, the lower in-

canopy velocity could produce comparable wave decay. We also expect diminished wave velocities within the meadow for the following cases: T5 (Aa_v=1.1), A4 (Aa_v=0.9), and A5 (Aa_v=1.0). Velocity measurements reported in *Luhar et al.* [2010] for these wave conditions show that orbital velocities within the meadow are reduced by as much as 21% compared to predictions made by linear wave theory.

Figure 7c shows the variation in wave decay over a range of wave periods (and also wavelengths). In general, decay decreased as the waves became shorter (period T decreases, kh increases). The decay per wavelength, $K_D a_0 \lambda$, was 0.11 (interpreted as an 11% reduction in wave height per wavelength) for waves of period 2.0 s (run T5) and only $K_D a_0 \lambda$=0.01 for waves of period 0.8 seconds (run T1). This is physically intuitive since shorter waves have velocities that decrease more rapidly with depth and smaller velocities within the meadow lead to reduced energy dissipation and wave decay. For example, linear wave theory (3) and (4) predicts that a wave of amplitude 5.0 cm in 39 cm water depth would produce a horizontal orbital velocity of 22 cm s^{-1} near the flume bed ($z = 0$ cm) for waves of period $T = 2.0$ s and only 5.6 cm s^{-1} for waves of period 0.8 s. Similarly, because velocity increases linearly with amplitude, we also expect higher wave decay for high-amplitude waves. This is confirmed by the wave decay measurements shown in Figure 7b. However, in both Figures 7b and 7c, the observed increase in wave decay with wave amplitude and period is not as steep as that predicted for rigid, upright blades. This may be explained by a decrease in effective blade length caused by higher velocities (and hence higher Cauchy number).

Finally, Figure 7d elucidates the impact of relative submergence. The water depth was varied between 16 cm (H1, l/h=0.8) and 39 cm (H4, l/h=0.3) while the wave period ($T = 1.4$ s) was kept constant for these runs. As a result, the parameters kh and l/h both varied for these experiments. The decay per wavelength, $K_D a_0 \lambda$, was 0.25 for case H1 with l/h=0.8. This reduced to $K_D a_0 \lambda$=0.09 for the case where l/h=0.3 (H4). In general, wave decay increased as the meadow occupied more of the water column [see also *Stratigaki et al.*, 2011; *Anderson and Smith*, 2014]. The predicted curve shown in Figure 7d suggests that decay is likely to be negligible if the meadow occupies less than 10% of the water column.

5. Discussion

5.1. Effective Length and Wave Decay

Figure 7 shows that the rigid blade assumption substantially overpredicts wave decay over the model canopy of flexible seagrass. Instead of calibrating the drag coefficient to account for the effect of vegetation motion, we propose the use of the physically motivated effective length framework. For the present experiments, the ratio of blade length to wave excursion was $L \geq 2.7$ and the Cauchy number was $Ca \geq 100$. Thus, we expect the high-forcing ($Ca \gg 1$) and small-excursion ($L \gg 1$) limit identified by *Luhar and Nepf* [2016] to apply. For this limit, the effective length is predicted to scale as $l_e/l \sim (CaL)^{-1/4}$ (12). As shown in Figure 8, the effective lengths estimated from blade motion imaging conform well to this predicted scaling law. (We also considered the large-excursion scaling, $l_e/l \sim Ca^{-1/3}$, shown in (11). However, this scaling did not lead to as good of a fit for the effective lengths, which is understandable given that it assumes $L \ll 1$.) Specifically, the following relationship provides the best fit to the data: l_e/l=2.25$(CaL)^{-1/4}$ (r^2=0.67). Importantly, this scaling law

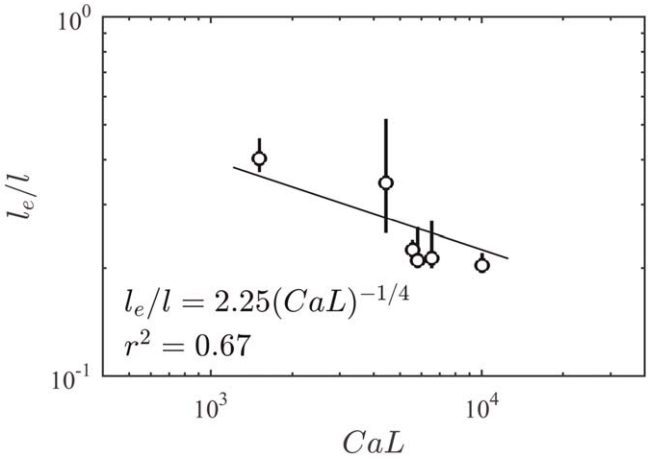

Figure 8. Estimated effective lengths from blade motion images l_e/l plotted against the product of the Cauchy number and the length ratio, CaL. The error bars reflect range of estimated effective lengths obtained by shifting the recorded blade motion by 1 phase bin (i.e., 1/15 of a second) relative to the linear wave-velocity field. The line shows the best fit power law with the exponent constrained to be $-1/4$.

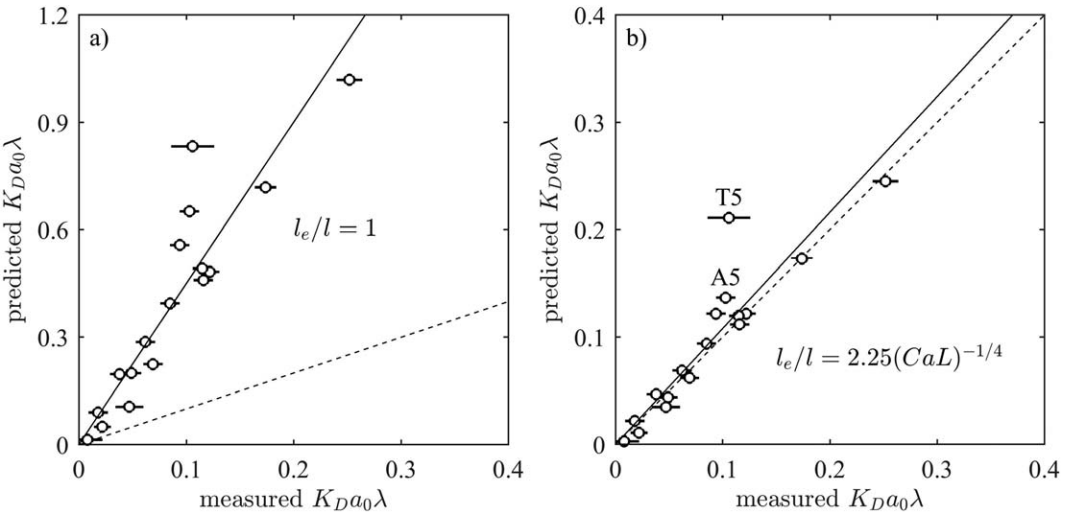

Figure 9. Measured and predicted wave decay for all the cases shown in Table 2. (a) Predictions assuming $l_e/l=1$. (b) Predictions assuming $l_e/l=2.25(CaL)^{-1/4}$, the best fit power law from Figure 8. The solid lines show the best fit linear relationships with zero intercept: the fitted slopes are 4.50 ($r^2=0.83$) for (a) and 1.08 ($r^2=0.84$) for (b). The dashed lines indicate perfect agreement.

is also consistent with the single blade data reported in *Luhar and Nepf* [2016], which were obtained via direct force measurements.

We next test whether the relation for effective length determined through video analysis of blade motion (Figure 8) can be used in (8) to predict observed wave decay. Figure 9 compares measured values for wave decay, $K_D a_0 \lambda$, with predictions made via (8). With the rigid blade assumption, $l_e = l$, the slope for the best fit linear relationship between predicted and measured wave decay is 4.50 (Figure 9a). In other words, the rigid blade assumption on average leads to a 350% overprediction of wave decay. Figure 9b shows that the predictions improve markedly when the effective blade length is calculated using the fitted relationship, $l_e/l=2.25(CaL)^{-1/4}$. Specifically, the slope for the best fit linear relationship is 1.08, i.e. an 8% overprediction on average. For most of the cases, the observed values are within 20% of the predictions, which further confirms that our physically-based model for effective length captures the behavior of the model seagrass blades well. There is one exception to the good prediction provided by the effective length. Specifically, wave decay is overpredicted substantially for run T5. As discussed above, for this case the wave excursion exceeds the drag length-scale ($Aa_v=1.1$), resulting in a reduction of in-canopy velocities [*Luhar et al.*, 2010] which is not accounted for in equation [8].

The results presented in Figure 9 show that the effective length framework successfully accounts for the effects of blade flexibility on wave-energy dissipation, providing an accurate prediction of measured wave decay. A major advantage of this approach is that it allows us to differentiate between the distinct physical phenomena that affect drag and energy dissipation. Specifically, the effects of shape and Reynolds number can be incorporated into the drag coefficient, so that C_D can be estimated from previous literature for rigid bluff body flows. The effects of vegetation bending and motion can be accounted for via the effective length l_e, which depends primarily on the Cauchy number Ca and length ratio L.

For field conditions, the Cauchy number Ca can be calculated based on estimates of the blade properties (width, length, thickness, and elastic modulus) and the significant wave height and peak period. However, the exact power law for l_e obtained here may not apply across all species of seagrass. Further, the broadband nature of waves in the field makes defining an effective length more difficult. Specifically, there could be multiple energetic wave frequencies in the field, and the vegetation is unlikely to dissipate all these frequencies equally, i.e., the canopy may act as a high-pass or low-pass filter for the waves [*Bradley and Houser*, 2009]. A single value for l_e identified from the significant wave height and peak period would not reproduce this frequency dependence, and so it may be necessary to define a frequency-dependent effective length [see also *Mullarney and Henderson*, 2010].

5.2. Vegetation Effects at the Regional Scale

Previous studies [*Gacia et al*., 1999; *Granata et al*., 2001] suggest that the reduction in wave-induced velocities within seagrass meadows results in lower local bed stresses. Lower bed stresses lead to reduced sediment resuspension and, therefore, enhanced particle retention. On a regional scale, the presence of seagrass can also impact the bed stresses by reducing the wave amplitude. We follow the methodology of *Fagherazzi et al*. [2006] to predict the reduction in wave amplitude over a vegetated region relative to a bare bed and hence, estimate the regional effects on near-bed velocity. We consider locally generated wind waves at equilibrium, such that the energy input from the wind is balanced by the energy extracted by bed friction in the absence of vegetation [as considered by *Fagherazzi et al*. [2006]), or by vegetative drag (as we now consider in comparison). For simplicity, we ignore energy losses associated with wave breaking and white capping, and we also ignore the influence of fetch, i.e., we consider an unlimited fetch. The dissipation rate due to bed friction is:

$$E_{D,bf} = 2\rho g C_{bf} a_{bf}^3 \omega \frac{k}{\sinh kh \ \sinh 2kh} \tag{16}$$

with bed friction coefficient, $C_{bf} = 0.015$ [*Fagherazzi et al*., 2006]. For conditions with only bed friction (*bf*) acting, we denote wave amplitude a_{bf}. Wave dissipation due to a seagrass meadow (repeated here for convenience) is as shown in (5)

$$E_{D,veg} = \frac{2}{3\pi} \rho C_D a_v \left(\frac{a_{veg}\omega}{\sinh kh}\right)^3 \left[\frac{9 \ \sinh kl_e + \sinh 3kl_e}{12k}\right]. \tag{17}$$

Here for conditions with vegetation we denote the wave amplitude as a_{veg}. Since we compare conditions at the same site, with and without seagrass, the wind input is the same. Therefore, we equate (16) and (17), and solve for the ratio a_{veg}/a_{bf} to compare the amplitude of waves in this region with and without vegetation. This ratio is given by the expression:

$$\left(\frac{a_{veg}}{a_{bf}}\right)^3 = \frac{3\pi}{2} \frac{C_{bf}}{C_D a_v l_e} \left[\frac{12kl_e}{9 \ \sinh kl_e + \sinh 3kl_e}\right]. \tag{18}$$

We compute this amplitude ratio for a typical seagrass meadow [see e.g., *Luhar et al*., 2010] subject to waves of period $T = 2.0$ s and $T = 8.0$ s. We assume that the seagrass blade length is $l = 0.5$ m, the water depth ranges from $h = 1$ m to $h = 10$ m, and the frontal area per unit volume ranges from $a_v = 1$ m^{-1} to $a_v = 10$ m^{-1}. Since the effective length depends on the local hydrodynamic forcing, it cannot be predicted independently of the wave amplitude a_{veg}. For simplicity, we assume a constant value of $l_e/l = 0.2$ such that $l_e = 0.1$ m. The drag coefficient is assumed to be $C_D = 1.95$.

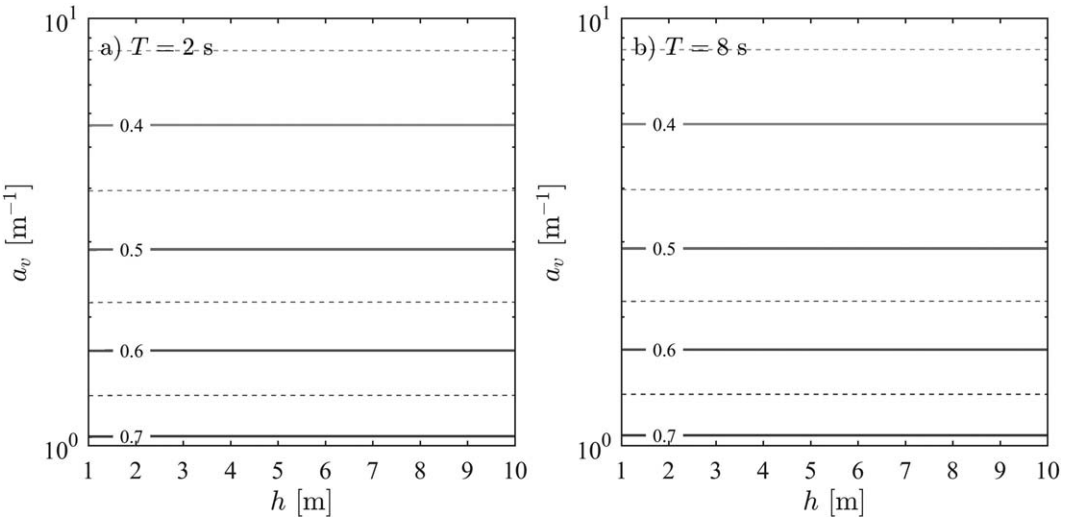

Figure 10. Contours showing ratio of steady state wave amplitudes over vegetated and bare beds a_{veg}/a_{bf} as a function of vegetation frontal area density a_v and water depth h. (a) Amplitude ratio for waves of period $T = 2$ s. (b) Amplitude ratio for waves of period $T = 8$ s.

As expected, the influence of seagrass on wave amplitude increases as vegetation density (a_v) increases (Figure 10). Recall from Figure 7 that wave decay increases as the fraction of the water column occupied by the vegetation increases (runs H4–H1) and decreases as the wave period decreases (runs T5–T1). However, Figure 10 shows that neither the wave period nor the water depth appreciably impact the amplitude ratio, a_{veg}/a_{bf}. This is because, for field conditions, the effective length of the vegetation is likely to be much smaller than the wavelength, $kl_e = 2\pi l_e/\lambda \ll 1$, and so the factor inside the square brackets in (18) is approximately equal to 1. At this limit, (18) simplifies to:

$$\frac{a_{veg}}{a_{bf}} \approx \left(\frac{3\pi}{2}\frac{C_{bf}}{C_D a_v l_e}\right)^{1/3}. \tag{19}$$

In other words, the wave period, wavelength, and water depth do not play a significant role. Instead, the parameter $C_{bf}/(C_D a_v l_e)$, which may be thought of as the ratio of energy dissipation over the two substrates, is the major control on the amplitude ratio.

Figure 10 shows that, for typical field conditions, the wave amplitude over a meadow is less than 70% of the amplitude over bare bed, i.e., a reduction of 30% or more. For dense meadows ($a_v \approx 10\ \mathrm{m}^{-1}$), the reduction in amplitude can be as large as 70%. Since wave-velocity scales linearly with wave amplitude, a similar reduction in near-bed velocity is expected. Thus, on a regional scale, wave decay due to seagrass meadows is likely to yield a significant reduction of near-bed velocities compared to regions without vegetation. Lower velocities lead to lower bed stresses, thereby reducing sediment re-suspension.

6. Conclusion

Through flume experiments, we have studied blade motion under waves and its impact on wave-energy dissipation over a seagrass meadow. Only relative motion between the blades and the water leads to hydrodynamic drag and hence, energy dissipation. As a result, the effective length of the seagrass blades, which approximates the length of blade over which relative motion between blades and water is significant, produces a better predictor of energy dissipation than models based on the full blade length. Consistent with recent experimental and theoretical research on the dynamics of flexible blades in oscillatory flows [*Mullarney and Henderson*, 2010; *Luhar and Nepf*, 2016], our results suggest that the effective blade length depends on the ratio of the restoring force due to blade rigidity and hydrodynamic drag (Cauchy number, *Ca*) as well as the ratio of blade length to wave excursion (*L*). Specifically, the ratio *CaL* provides a metric for predicting the effective blade length, l_e. The best fit to the data was a power law of the form $l_e/l = 2.25(CaL)^{-1/4}$. Using this estimator of the effective blade length, which was based on images of blade motion, we were able to predict the wave decay over the meadow. Previous researchers have simply used a calibrated value of the drag coefficient to account for blade motion. By studying the posture of the blades over a wave cycle, we give a mechanistic explanation for the lower drag coefficients.

We also studied the impact of vegetation characteristics (stem density and depth of submergence) and wave properties (period and amplitude) on wave decay. As anticipated, wave decay increases with increasing vegetation density (more drag-inducing elements). Relative depth of submergence also plays a major role; wave decay increases as the vegetation occupies a larger fraction of the water column. Further, wave decay decreases with decreasing wave period and increases with increasing wave height. This is because wave-induced velocities within the meadow increase as the wave period and wave height rise, and larger velocities lead to greater energy dissipation within the meadow. Finally, we show that on a regional scale, the amplitudes of steady state wind-generated waves over seagrass meadows could be less than 40% of the amplitudes over regions without vegetation because of energy dissipation due to vegetation drag.

Acknowledgments
This study received support from the US National Science Foundation under grants OCE 0751358 and EAR 1659923. Any conclusions or recommendations expressed in this material are those of the author(s) and do not necessarily reflect the views of the National Science Foundation. E. Infantes received financial support from Formas Grant Dnr. 231-2014-735. All data necessary to evaluate and build upon the work in this paper are available in the cited references, or are included in the figures and tables.

References

Alben, S., M. Shelley, and J. Zhang (2002), Drag reduction through self-similar bending of a flexible body, *Nature*, *420*(6915), 479–481.
Anderson, M. E., and J. Smith (2014), Wave attenuation by flexible, idealized salt marsh vegetation, *Coastal Eng.*, *83*, 82–92.
Asano, T., H. Deguchi, and N. Kobayashi (1992), Interaction between water waves and vegetation, in *Coastal Engineering Conference*, vol. 3, pp. 2710–2710, Am. Soc. Civ. Eng., New York.
Augustin, L. N., J. L. Irish, and P. Lynett (2009), Laboratory and numerical studies of wave damping by emergent and near-emergent wetland vegetation, *Coastal Eng.*, *56*(3), 332–340.

Bradley, K., and C. Houser (2009), Relative velocity of seagrass blades: Implications for wave attenuation in low-energy environments, *J. Geophys. Res.*, *114*, F01004, doi:10.1029/2007JF000951.
Chen, S.-N., L. P. Sanford, E. W. Koch, F. Shi, and E. W. North (2007), A nearshore model to investigate the effects of seagrass bed geometry on wave attenuation and suspended sediment transport, *Estuaries Coasts*, *30*(2), 296–310.
Coops, H., N. Geilen, H. J. Verheij, R. Boeters, and G. van der Velde (1996), Interactions between waves, bank erosion and emergent vegetation: An experimental study in a wave tank, *Aquat. Bot.*, *53*(3), 187–198.
Dalrymple, R. A., J. T. Kirby, and P. A. Hwang (1984), Wave diffraction due to areas of energy dissipation, *J. Waterway Port Coastal Ocean Eng.*, *110*(1), 67–79.
Duarte, C. M. (1991), Seagrass depth limits, *Aquat. Bot.*, *40*(4), 363–377.
Duarte, C. M., E. Benavent, and M. del Carmen Sánchez (1999), The microcosm of particles within seagrass *Posidonia oceanica* canopies, *Mar. Ecol. Prog. Ser.*, *181*, 289–295.
Ellington, C. (1991), Aerodynamics and the origin of insect flight, *Adv. Insect Physiol.*, *23*, 171–210.
Elwany, M. H. S., W. C. O'Reilly, R. T. Guza, and R. E. Flick (1995), Effects of southern California kelp beds on waves, *J. Waterway Port Coastal Ocean Eng.*, *121*(2), 143–150.
Eriander, L., E. Infantes, M. Olofsson, J. Olsen, and P.-O. Moksnes (2016), Assessing methods for restoration of eelgrass (*Zostera marina L.*) in a cold temperate region, *J. Exp. Mar. Biol. Ecol.*, *479*, 76–88.
Fagherazzi, S., L. Carniello, L. D'Alpaos, and A. Defina (2006), Critical bifurcation of shallow microtidal landforms in tidal flats and salt marshes, *Proc. Natl. Acad. Sci. U. S. A.*, *103*(22), 8337–8341.
Fonseca, M. S., and J. A. Cahalan (1992), A preliminary evaluation of wave attenuation by four species of seagrass, *Estuarine Coastal Shelf Sci.*, *35*(6), 565–576.
Fonseca, M. S., J. C. Zieman, G. W. Thayer, and J. S. Fisher (1983), The role of current velocity in structuring eelgrass (*Zostera marina L.*) meadows, *Estuarine Coastal Shelf Sci.*, *17*(4), 367–380.
Gacia, E., T. Granata, and C. Duarte (1999), An approach to measurement of particle flux and sediment retention within seagrass (*Posidonia oceanica*) meadows, *Aquat. Bot.*, *65*(1), 255–268.
Ghisalberti, M., and H. M. Nepf (2002), Mixing layers and coherent structures in vegetated aquatic flows, *J. Geophys. Res.*, *107*, 3-1–3-11, doi: 10.1029/2001JC000871.
Gijón Mancheño, A. (2016), Interaction between wave hydrodynamics and flexible vegetation, Master's thesis, TU Delft, Delft, Netherlands.
Gosselin, F., E. De Langre, and B. A. Machado-Almeida (2010), Drag reduction of flexible plates by reconfiguration, *J. Fluid Mech.*, *650*, 319–341.
Graham, J. (1980), The forces on sharp-edged cylinders in oscillatory flow at low Keulegan–Carpenter numbers, *J. Fluid Mech.*, *97*(2), 331–346.
Granata, T., T. Serra, J. Colomer, X. Casamitjana, C. Duarte, and E. Gacia (2001), Flow and particle distributions in a nearshore seagrass meadow before and after a storm, *Mar. Ecol. Prog. Ser.*, *218*, 95–106.
Hunt, J. (1964), The viscous damping of gravity waves in shallow water, *La Houille Blanche*, *6*, 685–691.
Infantes, E., A. Orfila, G. Simarro, J. Terrados, M. Luhar, and H. Nepf (2012), Effect of a seagrass (*Posidonia oceanica*) meadow on wave propagation, *Mar. Ecol. Prog. Ser.*, *456*, 63–72.
Keulegan, G. H., and L. H. Carpenter (1956), *Forces on Cylinders and Plates in an Oscillating Fluid*, U.S. Dep. of Comm., Natl. Bur. of Stand., Washington, D. C.
Knutson, P. L., R. A. Brochu, W. N. Seelig, and M. Inskeep (1982), Wave damping in *Spartina alterniflora* marshes, *Wetlands*, *2*(1), 87–104.
Kobayashi, N., A. W. Raichle, and T. Asano (1993), Wave attenuation by vegetation, *J. Waterway Port Coastal Ocean Eng.*, *119*(1), 30–48.
Koch, E. W., J. D. Ackerman, J. Verduin, and M. van Keulen (2006), Fluid dynamics in seagrass ecology: From molecules to ecosystems, in *Seagrasses: Biology, Ecology and Conservation*, edited by A. Larkum, R. J. Orth, and C. Duarte pp. 193–225, Springer, Netherlands.
Lowe, R. J., J. L. Falter, J. R. Koseff, S. G. Monismith, and M. J. Atkinson (2007), Spectral wave flow attenuation within submerged canopies: Implications for wave energy dissipation, *J. Geophys. Res.*, *112*, C05018, doi:10.1029/2006JC003605.
Luhar, M., and H. M. Nepf (2011), Flow-induced reconfiguration of buoyant and flexible aquatic vegetation, *Limnol. Oceanogr.*, *56*(6), 2003–2017.
Luhar, M., and H. Nepf (2016), Wave-induced dynamics of flexible blades, *J. Fluids Struct.*, *61*, 20–41.
Luhar, M., J. Rominger, and H. Nepf (2008), Interaction between flow, transport and vegetation spatial structure, *Environ. Fluid Mech.*, *8*(5–6), 423–439.
Luhar, M., S. Coutu, E. Infantes, S. Fox, and H. Nepf (2010), Wave-induced velocities inside a model seagrass bed, *J. Geophys. Res.*, *115*, C12005, doi:10.1029/2010JC006345.
Luhar, M., E. Infantes, A. Orfila, J. Terrados, and H. M. Nepf (2013), Field observations of wave-induced streaming through a submerged seagrass (*Posidonia oceanica*) meadow, *J. Geophys. Res. Oceans*, *118*, 1955–1968, doi:10.1002/jgrc.20162.
Madsen, O. S. (1971), On the generation of long waves, *J. Geophys. Res.*, *76*, 8672–8683.
Marbà, N., C. M. Duarte, E. Díaz-Almela, J. Terrados, E. Álvarez, R. Martínez, R. Santiago, E. Gacia, and A. M. Grau (2005), Direct evidence of imbalanced seagrass (*Posidonia oceanica*) shoot population dynamics in the Spanish Mediterranean, *Estuaries*, *28*(1), 53–62.
Méndez, F. J., and I. J. Losada (2004), An empirical model to estimate the propagation of random breaking and nonbreaking waves over vegetation fields, *Coastal Eng.*, *51*(2), 103–118.
Méndez, F. J., I. J. Losada, and M. A. Losada (1999), Hydrodynamics induced by wind waves in a vegetation, *J. Geophys. Res.*, *104*, 18,383–18,396.
Möller, I., T. Spencer, J. French, D. Leggett, and M. Dixon (1999), Wave transformation over salt marshes: a field and numerical modelling study from North Norfolk, England, *Estuarine Coastal Shelf Sci.*, *49*(3), 411–426.
Moore, K. A. (2004), Influence of seagrasses on water quality in shallow regions of the lower Chesapeake Bay, *J. Coastal Res.*, special issue 45, 162–178.
Mork, M. (1996), The effect of kelp in wave damping, *Sarsia*, *80*(4), 323–327.
Mullarney, J. C., and S. M. Henderson (2010), Wave-forced motion of submerged single-stem vegetation, *J. Geophys. Res.*, *115*, C12061, doi: 10.1029/2010JC006448.
Paul, M., T. Bouma, and C. Amos (2012), Wave attenuation by submerged vegetation: Combining the effect of organism traits and tidal current, *Mar. Ecol. Prog. Ser.*, *444*, 31–41.
Pergent-Martini, C., V. Rico-Raimondino, and G. Pergent (1994), Primary production of *Posidonia oceanica* in the Mediterranean Basin, *Mar. Biol.*, *120*(1), 9–15.
Peterson, C. H., R. A. Luettich Jr, F. Micheli, and G. A. Skilleter (2004), Attenuation of water flow inside seagrass canopies of differing structure, *Mar. Ecol. Prog. Ser.*, *268*, 81–92.

Riffe, K. C., S. M. Henderson, and J. C. Mullarney (2011), Wave dissipation by flexible vegetation, *Geophys. Res. Lett.*, *38*, L18607, doi:10.1029/2011GL048773.

Sánchez-González, J. F., V. Sánchez-Rojas, and C. D. Memos (2011), Wave attenuation due to *Posidonia oceanica* meadows, *J. Hydraul. Res.*, *49*(4), 503–514.

Stratigaki, V., E. Manca, P. Prinos, I. J. Losada, J. L. Lara, M. Sclavo, C. L. Amos, I. Cáceres, and A. Sánchez-Arcilla (2011), Large-scale experiments on wave propagation over *Posidonia oceanica*, *J. Hydraul. Res.*, *49*, suppl. 1, 31–43.

Vogel, S. (1994), *Life in Moving Fluids: The Physical Biology of Flow*, Princeton Univ. Press, Princeton, N. J.

Ward, L. G., W. M. Kemp, and W. R. Boynton (1984), The influence of waves and seagrass communities on suspended particulates in an estuarine embayment, *Mar. Geol.*, *59*(1–4), 85–103.